ORIGINAL PAPER

The peculiar heme pocket of the 2/2 hemoglobin of cold-adapted *Pseudoalteromonas haloplanktis* TAC125

Barry D. Howes · Daniela Giordano · Leonardo Boechi · Roberta Russo · Simona Mucciacciaro ·
Chiara Ciaccio · Federica Sinibaldi · Maria Fittipaldi · Marcelo A. Martí · Darío A. Estrin ·
Guido di Prisco · Massimo Coletta · Cinzia Verde · Giulietta Smulevich

Abstract The genome of the cold-adapted bacterium *Pseudoalteromonas haloplanktis* TAC125 contains multiple genes encoding three distinct monomeric hemoglobins exhibiting a 2/2 α-helical fold. In the present work, one of these hemoglobins is studied by resonance Raman, electronic absorption and electronic paramagnetic resonance spectroscopies, kinetic measurements, and different bioinformatic approaches. It is the first cold-adapted bacterial hemoglobin to be characterized. The results indicate that this protein belongs to the 2/2 hemoglobin family, Group II, characterized by the presence of a tryptophanyl residue on the bottom of the heme distal pocket in position G8 and two tyrosyl residues (TyrCD1 and TyrB10). However, unlike other bacterial hemoglobins, the ferric state, in addition to the aquo hexacoordinated high-spin form, shows multiple hexacoordinated low-spin forms, where either TyrCD1 or TyrB10 can likely coordinate the iron. This is the first example in which both TyrCD1 and TyrB10 are proposed to be the residues that are alternatively involved in heme hexacoordination by endogenous ligands.

Keywords Resonance Raman · EPR · Molecular dynamics · Tyrosinate ligand · Antarctic bacterium

D. Giordano and L. Boechi contributed equally to this work.

B. D. Howes · S. Mucciacciaro · M. Fittipaldi ·
G. Smulevich (✉)
Dipartimento di Chimica, Università di Firenze,
50019 Sesto Fiorentino (FI), Italy
e-mail: giulietta.smulevich@unifi.it

M. Fittipaldi
INSTM (Consorzio Interuniversitario per la Scienza
e Tecnologia dei Materiali), 50019 Sesto Fiorentino (FI), Italy

D. Giordano · R. Russo · G. di Prisco · C. Verde
Institute of Protein Biochemistry,
CNR, 80131 Naples, Italy

L. Boechi · M. A. Martí · D. A. Estrin
Departemento de Química Inorgánica,
Analítica y Química Física/INQUIMAE-CONICET,
Facultad de Ciencias Exactas y Naturales,
Universidad de Buenos Aires,
C1428EHA Buenos Aires, Argentina

C. Ciaccio · F. Sinibaldi · M. Coletta
Dipartimento di Medicina Sperimentale e Scienze Biochimiche,
Università di Roma Tor Vergata, 00133 Rome, Italy

C. Ciaccio · M. Coletta · G. Smulevich
Consorzio Interuniversitario di Ricerca in Chimica dei Metalli
nei Sistemi Biologici, 70126 Bari, Italy

Introduction

Most ocean waters are permanently at temperatures ranging between 2 and 4 °C. Therefore, marine organisms have been exposed to a permanent excess of oxygen, due to the high solubility of this gas at cold temperatures, leading to oxygen reserves that are larger than those available in warmer waters. Although many cold-adapted marine species have been studied [1], we still have limited knowledge about molecular adaptations at low temperatures. The genome of the Antarctic marine eubacterium *Pseudoalteromonas haloplanktis* TAC125 (*Ph*TAC125) has been sequenced and annotated [2], shedding light on several molecular features that have selectively developed in cold environments. The genome contains multiple genes encoding three different truncated hemoglobins (Hbs) at distinct positions on chromosome I, namely *PSHAa0030*, *PSHAa2217* and *PSHAa0458*, which exhibit a 2/2 α-helical fold [3]. The unusually high number of 2/2 Hbs strongly suggests that these proteins are bound to fulfil important physiological roles that are perhaps related to the peculiar features of the Antarctic habitat.

In the present study, we cloned and overexpressed the 2/2 Hb encoded by the *PSHAa0030* gene (hereafter named *Ph*-2/2HbO). The ferric form was investigated by spectroscopy, kinetic measurements and different computer simulation approaches. This work represents the first detailed characterization of a cold-adapted bacterial Hb. The results highlight the unique features of the ferric state among 2/2 Hbs of Group II. The ensemble of results indicates high protein structural flexibility, which may be linked to the cold environment.

Materials and methods

Protein expression and purification

The gene encoding *Ph*-2/2HbO was cloned as described previously [3]. The reported expression and purification methods were replaced by an alternative procedure to (a) improve the biomass yield of *Ph*-2/2HbO, and (b) avoid sulfide binding [4].

Using the previous purification procedure, in the presence of 1.0 mM β-ME, *Ph*-2/2HbO was isolated in a ferric form with a Soret band at 427 nm and a broad band at 550 nm. The close similarities of this unusual spectrum to that of sulfide-bound heme proteins suggested that an exogenous sulfide ligand was bound to the heme Fe atom [4–6], possibly derived from sulfide impurities contained in β-ME used during the purification steps. Accordingly, in the present work, in the absence of β-ME, ferric *Ph*-2/2HbO displays quite different spectral

characteristics (see Fig. S1 of the Electronic supplementary material, ESM).

The strain BL21(DE3) of *Escherichia coli* was successfully transformed with the recombinant expression plasmid pET28a-2/2HbO. The cells were grown overnight in a flask at 37 °C and shaken at 180 rpm. Fifty microliters of the growth medium were inoculated in an Applikon fermentor with a working volume of 1 l. The culture was grown using a mineral medium according to a standard procedure from CPC Biotech. The first growth phase occurred in fed-batch mode at 30 °C. After 23 h, the temperature was decreased to 25 °C. The culture was induced at $OD_{600} = 32$ by the addition of isopropyl-1-thio-D-galactopyranoside to a final concentration of 0.5 mM, and 0.3 mM δ-aminolevulinic acid; expression was continued overnight. The cells were harvested by centrifugation at 4 °C.

For purification, the frozen cells were thawed, suspended in 50 mM Tris–HCl pH 7.6, 1.0 mM EDTA, 1.0 mM phenylmethylsulfonylfluoride and protease-inhibitor cocktail (SIGMA P8465) and disrupted in a French press until the supernatant was reddish and clear. The cell debris was removed by centrifugation at 30,000 rpm for 1 h at 4 °C. The supernatant was loaded onto an anion-exchange column (Q Sepharose Fast Flow, GE Healthcare Biosciences), equilibrated with 20 mM Tris–HCl pH 7.6 and 1.0 mM EDTA (Akta Explorer system, GE Healthcare Biosciences, Amersham Biosciences Ltd, UK). *Ph*-2/2HbO was eluted with a NaCl gradient (from 0 to 0.25 M) in 20 mM Tris–HCl pH 7.6, 1.0 mM EDTA [3]. The fraction was chosen on the basis of the absorbance of heme at 407 nm and protein at 280 nm. The collected protein was concentrated, dialyzed against 50 mM 2-(*N*-morpholino)ethanesulfonic acid (MES) pH 6.0, and further purified with a SP (sulfopropyl) Sepharose Fast Flow column (GE Healthcare Biosciences) equilibrated with 50 mM MES pH 6.0. The protein was eluted with a NaCl gradient (from 0 to 0.35 M). Final purification was performed by using another strong cation-exchange column, Mono S (GE Healthcare Biosciences) equilibrated with 50 mM MES pH 6.0 and applying a NaCl gradient (from 0 to 0.50 M). The protein obtained was over 98% pure, as judged from sodium dodecyl sulfate polyacrylamide gel electrophoresis (SDS-PAGE), and was stored at −20 °C. The N-terminal sequence was elucidated by automatic sequencing performed with an Applied Biosystems Procise 494 Automatic Sequencer, equipped with on-line detection of phenylthiohydantoin amino acids.

Sample preparation

The samples of *Ph*-2/2HbO at pH 5.6 and 7.6 were prepared in 0.1 M MES and 0.1 M Tris–HCl or 0.1 M

3-morpholinopropane-1-sulfonic acid (MOPS) buffers, respectively. Protein concentrations in the range 10–70 μM were used for the electronic absorption and RR samples. Sample concentration for low-temperature RR was between 30 and 100 μM. For kinetics measurements, the final protein concentration was 5 μM. The concentration of the electron paramagnetic resonance (EPR) sample was 160 μM. The protein concentration was determined on the basis of the molar absorptivity, $\varepsilon = 131$ mM^{-1} cm^{-1} at 408 nm.

Electrochemistry

Direct current cyclic voltammetry was carried out at 25 °C using an AMEL (Milan, Italy) 433 multipolarograph. A saturated calomel electrode (+244 mV vs. NHE at 25 °C; AMEL) was the reference electrode and a pyrolytic graphite electrode was the working electrode (3-mm diameter, AMEL), modified as previously described [7]. Cyclic voltammograms were run at 25 °C in the potential range +200 to −600 mV (vs. the standard calomel electrode), at scan rates of 0.05–1.00 V/s. Measurements were carried out in 0.1 M phosphate pH 7.0.

Spectroscopy

Electronic absorption spectra were measured with a double-beam Cary 5 spectrophotometer (Varian, Palo Alto, CA, USA) using a 5-mm NMR tube and a 600 nm min^{-1} scan rate. The RR spectra were obtained using a 5-mm NMR tube and by excitation with the 406.7, 530.9 and 568.2 nm lines of a Kr$^+$ laser (Innova 300 C, Coherent, Santa Clara, CA, USA), and the 496.5 and 514.5 nm lines of an Ar$^+$ laser (Innova 90/5, Coherent). A detailed description of the room and low-temperature RR experimental procedures has been reported previously [8]. The measurements at 4 °C were obtained using a thermostatically controlled water bath. All RR measurements were repeated several times under the same conditions to ensure reproducibility. The RR spectra were calibrated with indene and CCl$_4$ as standards to an accuracy of 1 cm^{-1} for intense isolated bands. The RR spectrum of water was subtracted from all spectra obtained with excitation at wavelengths in the visible region (496.5–568.2 nm). Spectra in polarized light were obtained by inserting a Polaroid analyzer between the sample and the entrance slit of the monochromator. The depolarization ratios, $\rho = I_\perp / I_{//}$, of the bands at 314 and 460 cm^{-1} of CCl$_4$ were measured to check the reliability of the polarization measurements. The values obtained, 0.73 and 0.00, respectively, compare well with the theoretical values of 0.75 and 0.00. To determine peak intensities and positions, a curve-fitting program (Lab Calc, Galactic) was used to simulate experimental spectra, using a Lorentzian line shape. The frequencies of the bands were optimized with an accuracy of 1 cm^{-1}, and the bandwidths with an accuracy of 0.5 cm^{-1}.

EPR spectra were recorded as reported previously [8].

Kinetic measurements were carried out employing a rapid-mixing stopped flow (SX.18MV, Applied Photophysics, Salisbury, UK) with a 1 ms dead time. The Fe(III) form of Ph-2/2HbO was mixed with different concentrations of sodium azide in 0.1 M phosphate buffer pH 7.0 at 20 °C, and transient absorption spectra were collected between 350 and 700 nm. Kinetic progress curves were fitted according to the following equation:

$$OD_{obs} = OD_{t=\infty} \pm \sum_{i=1}^{i=n} \Delta OD_i \exp^{(-ik_{obs}t)}, \tag{1}$$

where OD_{obs} is the absorption at 408 nm at a given time from the start of the reaction, OD_∞ is the absorption at longer times from the start of the reaction (when it is completed), ΔOD_i is the signal change for phase i, k_i is the rate constant for phase i, and t is time. The sign $\pm$ indicates that, depending on the wavelength, the signal may either decrease or increase.

Sequence alignment

Sequence alignments were performed between Ph-2/2HbO and four Hbs belonging to Group II for which the crystal structures are available, namely Mycobacterium tuberculosis (Mt-2/2HbO) (pdb Id: 1NGK), Bacillus subtilis (Bs-2/2HbO) (1ux8), Geobacillus stearothermophilus (Gs-2/2HbO) (2bKm), Thermobifida fusca (Tf-2/2HbO) (2bMM). Shewanella oneidensis 2/2HbO (see Fig. S2 of the ESM) was selected due to the presence of an extension at the N-terminus of the primary structure, similar to Ph-2/2HbO. Sequence identities are 34, 37, 34, 33 and 39%, respectively.

To align these sequences, different computational programs have been used, namely Modeller [9], BLAST [10] and ClustalX [11]. Based on the present and previous alignments [3], we constructed 3D models using Mt-2/2HbO and Bs-2/2HbO proteins as templates, and the Modeller program with default parameters. Several putative Ph-2/2HbO structures were obtained.

Molecular dynamics simulations

To evaluate the stabilities of the different structures, molecular dynamics simulations (MD) were performed for each structure using the Amber 9 force field ff99SB [12]. Initially, every system was minimized to avoid any possible structural clashes. Subsequently, the systems were

heated slowly from 0 to 300 K using a time step of 0.1 fs, and with a constraint on the α-C of the protein backbone. A short simulation at the constant temperature of 300 K under a constant pressure of 1 bar was then performed using a time step of 0.1 fs to allow the systems to reach proper density, as shown previously [13, 14]. Finally, 2 ns of MD using a time step of 2 fs was performed for each structure. The majority of the structures were found to be unstable and unfolded during the time scale of these short simulations. The most stable structure was obtained by using the X-ray structure of *Bs*-2/2HbO as a template and sequence alignments with ClustalX. This model structure was used to perform 40 ns of MD simulation. The structure was found to be stable during the time scale of the simulation (Fig. S3 of the ESM).

To build the Tyr hexacoordinated structures, we pushed the tyrosine oxygen toward the Fe(III) atom until typical binding distances were reached, and we used the generated structure to start a new simulation with TyrO⁻ coordinated to Fe(III), including the Fe–TyrO⁻ bond in the force field. We carried out minimization and thermalization as described above, and 20 ns of MD were performed for the protein with TyrCD1-O⁻ and with TyrB10-O⁻ coordinated to Fe(III). The charges and parameters of the active site were determined as reported previously [15] using the isolated heme with a coordinated Tyr-O⁻ as the model at the DFT/B3LYP level with a 6-31G** basis set to compute the active-site electronic structure. Since no reliable structural information can be obtained for the pre-A helix, all simulations were performed without this motif at the N-terminus.

Results

Sequence alignment

The sequence alignment indicates that *Ph*-2/2HbO has structural features typical of 2/2 Hbs, and especially those belonging to Group II. In particular, *Ph*-2/2HbO has Trp at position G8, and both the CD1 and the B10 positions are occupied by Tyr (see Fig. S2 of the ESM). These three positions are the most important for oxygen stabilization in this family of Hbs [16]. In contrast to Group I of 2/2 Hbs, the E7 and E11 positions are occupied by nonpolar amino-acid residues, Ile and Phe, respectively, precluding ligand stabilization by these two residues.

Several structures of *Ph*-2/2HbO were obtained (see "Materials and methods") starting from different alignments, with proteins of Group II giving rise to different initial structural models. The global fold of the models was very good, and the most significant structural differences were located in the CD loop, due to the insertion of three residues (Figs. S2, S4 of the ESM). In all of the obtained alignments, the important heme cavity residues (HisF8, TyrB10, TrpG8, TyrCD1, IleE7, PheE11) are in the positions originally proposed by Wittenberg et al. [17] and subsequently confirmed by Vuletich and Lecomte [18] for Group II proteins.

This alignment differs from that obtained in a previous study with other Group II proteins, where the residue at CD1 was His [3]. The latter did not take into account the insertion of three residues in the CD loop, so the CD loop of the current alignment is longer than in other Group II Hbs.
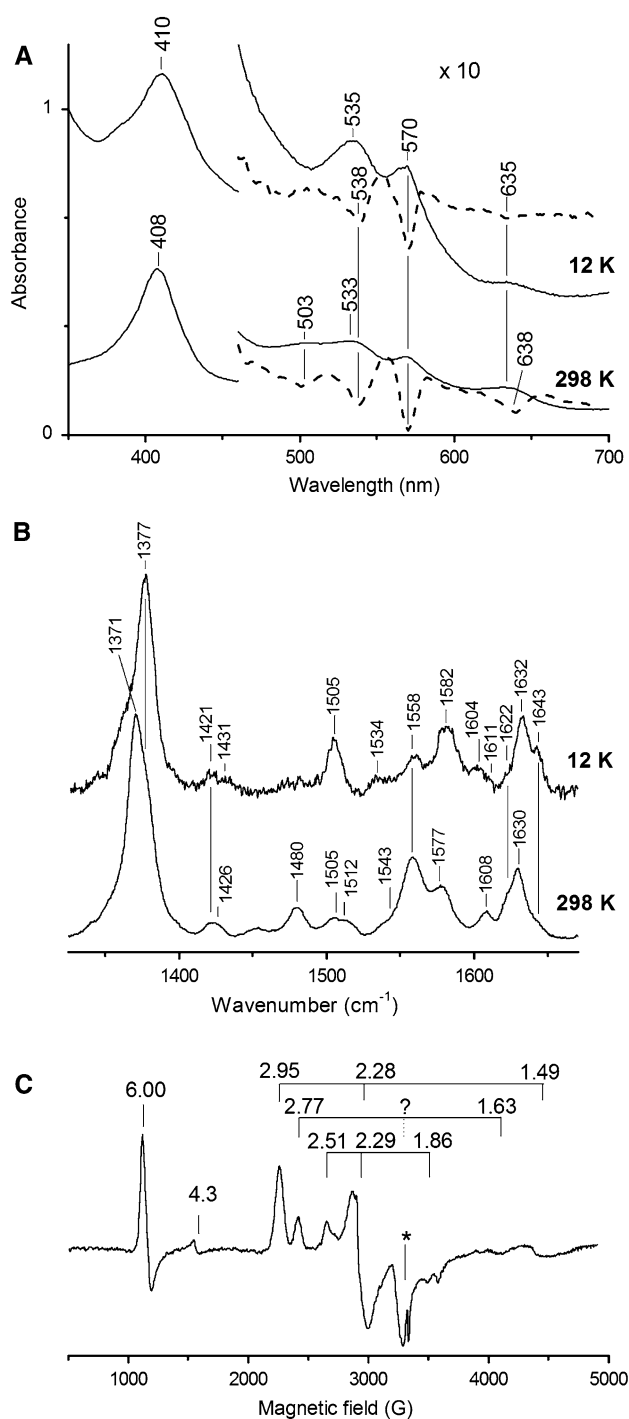
Redox potential measurements

The redox potential of *Ph*-2/2HbO at pH 7.0 [(−80 mV vs. standard hydrogen electrode (SHE)] is low compared to that of horse heart myoglobin (Mb) and human Hb (+50 and +135 mV, respectively) [19].

Spectroscopy at room temperature

The electronic absorption spectrum of ferric *Ph*-2/2HbO and its second-derivative spectrum (D^2, dotted line) are invariant over the pH range 5.6–7.6. The spectrum obtained at pH 7.6 (Fig. 1a, bottom) is characterized by a Soret band at 408 nm and bands in the visible region at 503, 533 (538 in D^2), 570, and 635 nm (638 in D^2). The wavelength maxima suggest the presence of various species, namely a His–Fe–H₂O six-coordinate high-spin (6cHS) form [bands at 503 and charge-transfer transition (CT1) at 635 nm] and at least one 6c-low-spin (LS) heme (bands at 533 and 570 nm). The absorption maxima of the LS forms are quite unusual, reminiscent of those of ferric *Chlamydomonas* Hb [20] and the hemophore HasA proteins from *Serratia marcescens* and *Pseudomonas aeruginosa* [21, 22], and they are very different from either a LS His–Fe–His (that exhibits well-defined absorption bands at about 535 and 565 nm) or a His–Fe–OH heme complex (that exhibits well-defined absorption bands at about 540 and 580 nm) [23]. Therefore, on the basis of the similarity with the UV–vis spectrum of ferric *Chlamydomonas* Hb and HasA hemophores, a His and a Tyr ligand are suggested to occupy the fifth and sixth coordination positions, respectively.

In agreement with the electronic absorption spectra, the Raman excitation profile at pH 7.6 (Fig. 1b, bottom; Fig. S5 of the ESM), together with the spectra in polarized light (Fig. 2b), allow the identification of three species: a 6cHS species (v_3 at 1,480 cm⁻¹, v_{10} at 1,608 cm⁻¹), and two 6cLS species. In particular, with Soret excitation, two 6cLS v_3 bands at 1,505 and 1,512 cm⁻¹ were observed (Fig. 1b, bottom; Fig. S5 of the ESM; Fig. 2b, bottom trace), and in the 1,600–1,650 cm⁻¹ region the spectra in polarized light

these bands are also observed in Q band excitation. This is consistent with previous observations for various heme containing peroxidases—namely CcP [24], HRPC [25], and *Coprinus cinereus* peroxidase (CIP) [26]—despite the fact that vinyl stretching modes are not expected to be enhanced a priori with visible excitation. The complete assignment of the high-frequency region is reported in Table S1 of the ESM.

A Tyr coordinated to a heme iron can often be identified by RR experiments. In fact, excitation in the tyrosinate–Fe(III) CT band (near 500 nm) yields characteristic vibrational frequencies of the bound phenolate [27]. In the 400–1,700 cm^{-1} region, the spectra taken with excitation wavelengths in the visible region (Fig. 2a; Fig. S5 of the ESM) clearly show the enhancement of two bands at 598 and 1,510 cm^{-1} (which are polarized, data not shown), displaying maximum intensification for excitation at 514.5 nm. Figure 2a shows the two spectral regions expanded to better visualize the bands. These bands are assigned to the v(Fe–O$_{Tyr}$) and v_{Tyr}(C=C) tyrosinate modes, respectively. Note that, despite the observation of two low-spin forms in the RR spectra, only one v(Fe–O$_{Tyr}$) stretching mode at 598 cm^{-1} is clearly evident. However, we cannot exclude that a second mode is hidden under the polarized band at 572 cm^{-1} observed in both Soret and visible excitations (Fig. 2a; Fig. S5 of the ESM), assigned to the v_{48} (E_u) in analogy to Mb [28].

The frequencies of the phenolate modes observed for a number of heme iron–tyrosinate proteins are listed in Table 1 [20, 29–34]. In general, ferric–heme proteins with tyrosinate ligation have been found to have penta- or hexa-HS heme states. The only exceptions are *Chlamydomonas* Hb and the HasA hemophores, which have 6cLS hemes. The tyrosinate 6cLS heme of the protein studied herein, *Ph*-2/2HbO, is now added to this list. Table 1 shows that while the v_{Tyr}(C=C) modes occur in a narrow frequency range, the v_{Tyr}(C–O) and v(Fe–O$_{Tyr}$) modes are markedly variable, ranging from 1,260 to 1,310, and from 502 to 623 cm^{-1}, respectively. The comparison between the data

enable the identification of two polarized bands at 1,622 and 1,630 cm^{-1} assigned to the v(C=C) vinyl stretching modes (Fig. 2b, bottom trace). Upon excitation with the 514.5 nm line (i.e., in resonance with the visible bands), two depolarized bands at 1,635 and 1,643 cm^{-1} were identified and assigned to two v_{10} modes of 6cLS hemes (Fig. 2b). The v(C=C) vinyl stretching modes are enhanced via the A-term (Franck–Condon mechanism); however,

Fig. 2 RR spectra of ferric *Ph*-2/2HbO at 298 K, in 20 mM Tris–HCl, pH 7.6 obtained with various excitation wavelengths: 406.7 nm, 10 mW laser power at the sample, 1 cm^{-1} spectral resolution; 413.1 nm, 15 mW laser power at the sample, 1 cm^{-1} spectral resolution; 496.5 nm, 100 mW laser power at the sample, 2.4 cm^{-1} spectral resolution; 514.5 nm, 150 mW laser power at the sample, 2.2 cm^{-1} spectral resolution; 530.9 nm, 36 mW laser power at the sample, 2.5 cm^{-1} spectral resolution; 568.2 nm, 23 mW laser power at the sample, 2 cm^{-1} spectral resolution and in polarized light at room temperature. a Experimental conditions: 413.1 nm, average of 18 spectra with 180 s integration time; 496.5 nm, average of 4 spectra with 720 s integration time; 514.5 nm, average of 15 spectra with 720 s integration time; 530.9 nm, average of 15 spectra with 600 s integration time (low frequency) and average of 6 spectra with 720 s integration time (high frequency); 568.2 nm, average of 7 spectra with 600 s integration time. The 520–740 cm^{-1} region has been expanded twofold. The intensities are normalized to that of the 1,230 cm^{-1} band (v_{13}). b RR spectra in polarized light taken with excitation wavelengths at 406.7 and 530.9 nm in 0.1 M MOPS and with excitation wavelengths at 496.5 and 514.5 nm in 20 mM Tris–HCl at pH 7.6. Experimental conditions: 406.7 nm, average of 8 spectra (*continuous line*, parallel, //) and of 27 spectra (*dotted line*, perpendicular, ⊥) with 600 s integration time; 496.5 nm, average of 5 spectra (//) and of 8 spectra (⊥) with 720 s integration time; 514.5 nm, average of six spectra (//) and of 8 spectra (⊥) with 720 s integration time; 530.9 nm, average of 12 spectra (//) and of 13 spectra (⊥) with 600 s integration time. The intensities are normalized to that of the 1,230 cm^{-1} band (v_{13})

reported in Table 1 for various heme proteins allows us to exclude a trans-axial effect altering the frequencies of these latter modes. However, different factors can affect these frequencies, namely (a) the TyrO–Fe bond angle via the interaction between the π orbitals of phenolate and the porphyrin, (b) the relative orientation between the tyrosinate ring and the heme plane, and (c) the Fe–O bond strength via the donation of electrons from phenolate to the heme with consequent weakening of the Fe–O bond. Formation of H-bonds between the tyrosinate and neighboring groups strongly affects the frequency of the v(Fe–O$_{Tyr}$) modes. In the 6cLS *Chlamydomonas* Hb, the band at 502 cm^{-1} was assigned to a tyrosinate H-bonded to a Lys residue. Recently, for the natural mutant, Hb M Saskatoon, in which the distal E7 His is replaced by a Tyr residue giving rise to a 6cHS species, two v(Fe–O$_{Tyr}$) modes at 581 and 598 cm^{-1} have been observed (Table 1) [34]. These bands were assigned to a Fe–O (protonated Tyr) (581 cm^{-1}) and a Fe–O (deprotonated Tyr) (598 cm^{-1}) stretching mode, respectively, on the basis of variations in their relative intensities at alkaline pH. The frequency of 598 cm^{-1} is close to the Fe–(deprotonated Tyr) stretching frequency of another natural Hb mutant, Hb M Boston (603 cm^{-1}) [30], and identical to that reported herein for the v(Fe–O$_{Tyr}$) mode. This outstanding coincidence of frequencies suggests that, for at least one of the LS forms observed in the RR spectra, the heme-bound *Ph*-2/2HbO distal Tyr residue corresponds to a deprotonated species at pH 7.6.

Azide binding kinetics

Figure 3a shows the progress curves at 408 nm for sodium azide binding to ferric *Ph*-2/2HbO at pH 7.0 and 20 °C. The continuous lines correspond to the nonlinear least-squares fitting of the data according to Eq. 1, employing three exponentials (i.e., $i = 3$ in Eq. 1).

In particular, two of these exponentials correspond to azide-dependent bimolecular processes, whereas a third process displays a rate which does not seem to depend on azide concentration. As is evident from Fig. 3a, the optical density change resulting from the reaction with azide increases as the concentration is increased. The ΔOD at 408 nm for the two bimolecular processes is reported in Fig. 3b as a function of azide concentration. Optical density changes were analyzed according to the following equation:

$$\Delta OD_{obs} = \Delta OD_{tot} \frac{K[N_3^-]}{1 + K[N_3^-]}, \tag{2}$$

where ΔOD_{obs} is the optical density change at 408 nm corresponding to the exponential process, ΔOD_{tot} is the total optical density change at 408 nm (corresponding to

Table 1 Tyrosinate vibrational bands (cm^{-1}) for ferric heme proteins with tyrosinate ligation

Protein	Spin state	ν_{Tyr}(C=C)	ν_{Tyr}(C=C)	ν_{Tyr}(C–O)	ν(Fe–O$_{Tyr}$)	Reference
Ph-2/2HbO	6cLS	1,601[a]	1,510	n.d.[b]	598	This work
Chlamydomonas Hb	6cLS	1,595	1,500	1,308	502	20
Hb M Saskatoon	6cHS	1,607	1,504	1,300	581/598	29, 30, 34
Hb M Boston	5cHS	1,603	1,504	1,279	603	29, 30
Human Mb (H93Y)	5cHS	1,603	1,504	1,302	585	31
Human HO-1(H25Y)	5cHS	1,605	1,504	1,258	591	32
ShuT	5cHS	1,601	1,502	1,301/1,265	613	33

[a] This band overlaps with the 6cHS ν_{10} observed at 1,608 cm^{-1}. A polarized band at 1,601 cm^{-1} has been observed by curve fitting (bandwidth 13 cm^{-1}) the spectra obtained with 514.5 nm excitation in polarized light (data not shown)

[b] This band overlaps with a mode observed at 1,309 cm^{-1} and assigned to the ν_{21} (see Table S1 of the ESM)

complete saturation of the binding site), K is the equilibrium constant, and [N$_3^-$] is the azide concentration. In this way, it was possible to determine the apparent equilibrium constant of azide binding to the two Fe(III) forms of *Ph*-2/2HbO, which are characterized by the two bimolecular processes (corresponding to $K = 9.8 \pm 1.2 \times 10^1$ M^{-1} for the faster bimolecular process 1, and $K = 5.5 \pm 0.7 \times 10^2$ M^{-1} for the slower bimolecular process 2, respectively). This information is particularly important since it allows the concentration dependence of the two bimolecular rate constants (Fig. 3c) to be fitted in a constrained way with physically meaningful parameters. In this respect, the ligand concentration dependence of kinetic rate constants has been fitted using a classical bimolecular scheme:

$$k_{obs} = k_{on}[N_3^-] + k_{off}. \qquad (3)$$

The nonlinear least-squares fitting of the two bimolecular rate constants is reported in Fig. 3c. It is noted that only for the faster bimolecular process does the use of Eq. 3 give a satisfactory description of the azide-concentration dependence, with values of k_{on} (=2.4 $\pm$ 0.3 $\times$ 10^2 M^{-1} s^{-1}) and k_{off} (=2.44 $\pm$ 0.38 s^{-1}) compatible with the value of K [=9.8($\pm$1.2) $\times$ 10^1 M^{-1}] obtained from optical density changes (Fig. 3b). In the case of the slower bimolecular rate constant, we must use a different reaction scheme (Scheme S1 of the ESM). The nonlinear least-squares fits of the rates for the two bimolecular processes are reported in Fig. 3c; the corresponding parameters are reported in Table 2.
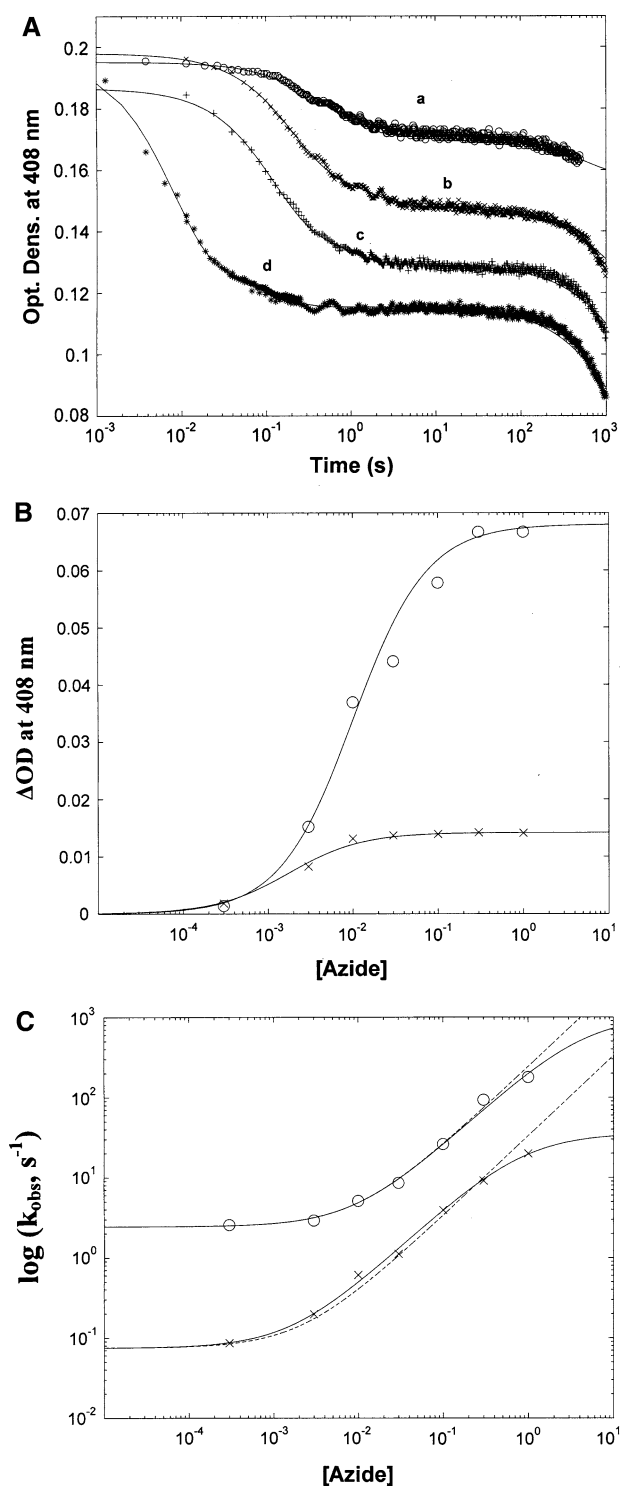
Clearly, the fact that these data need three exponentials indicates that the azide ligand encounters three different hexacoordinated forms in the heme pocket. Two of these forms allow a fairly fast ligand binding, such that the process maintains its bimolecular nature (probably because the originally bound ligand dissociates quickly), whereas the third one, which is the slowest concentration-independent process, seems to reflect a situation where the heme Fe(III) atom is hexacoordinated by a ligand which dissociates very

slowly (with a $k_{obs} \cong 7.0 \pm 1.5 \times 10^{-4}$ s^{-1}), such that the dissociation process is rate limiting under all conditions [i.e., when $k_2' \cdot$ [N$_3^-$] $\gg k_1'$, k_1; see Scheme S1 of the ESM].

Spectroscopy at low temperature

The electronic absorption and the D^2 spectra of ferric *Ph*-2/2HbO in the low-temperature range 220–12 K (Fig. 1a, top) are essentially those of 6cLS hemes. The LS Q-bands observed at room temperature (535 and 570 nm) are intensified, whereas the Soret band redshifts by 2 nm and the 6cHS bands at 503 and 635 nm (638 nm in the D^2 spectrum) are considerably reduced. In accord with the low-temperature absorption spectrum, the high-frequency RR spectrum at 12 K pH 7.6 shows an intensification of the LS form (ν_3 1,505, ν_2 1,582, ν_{10} 1,643 cm^{-1}) at the expense of the 6cHS form (ν_3 1,480, ν_2 1,558, ν_{10} 1,608 cm^{-1}) observed at 298 K (Fig. 1b), which is considerably reduced at 12 K. Moreover, of the two LS forms observed at 298 K, characterized by ν_3 bands at 1,505 and 1,512 cm^{-1}, only one form appears to be particularly enhanced at 12 K (ν_3 at 1,505 cm^{-1}). Interestingly, at the physiological temperature for the bacterium (4 °C), a slight increase in the relative intensity of the RR ν_3 LS band at 1,505 with respect to that at 1,512 cm^{-1} has been observed, together with an intensification (of ca. 20%) of the UV–vis Soret band (Fig. S6 of the ESM). Nevertheless, the broad ν_2 band (1,582 cm^{-1}) at 12 K suggests the presence of two LS forms. This interpretation is supported by the presence of the bands at 1,604 and 1,611 cm^{-1}, assigned to two ν_{37} LS modes.

X-band EPR spectroscopy (at 5 K) was carried out to gain further insight into the spin state and heme coordination environment of the protein (Fig. 1c). In agreement with the electronic absorption and RR spectra, the EPR spectrum at pH 7.6 is characterized by an axial HS ferric signal ($g_\perp \sim 6.0$, $g_\parallel \sim 2.0$) and three rhombic LS forms:

◀ **Fig. 3** **a** Kinetic progress curves at 408 nm of 3×10^{-6} M Fe(III) *Ph*-2/2HbO for different concentrations of N_3^-; i.e., 3×10^{-4} M (*curve a*), 3×10^{-3} M (*curve b*), 1×10^{-2} M (*curve c*) and 3×10^{-1} M (*curve d*) at pH 7.0 and 20 °C. *Continuous lines* represent nonlinear least-squares fits to data employing Eq. 1 with three exponentials (i.e., $i = 3$ in Eq. 1). **b** Amplitude of optical-density changes at 408 nm for the first two exponentials (*open circle r*1 and *asterisk r*2) of N_3^- binding to 3×10^{-6} M Fe(III) *Ph*-2/2HbO as a function of $[N_3^-]$. *Continuous lines* show nonlinear least-squares fits to data employing Eq. 2. **c** Dependence on $[N_3^-]$ of the observed rate constants for the first two exponentials of azide binding to Fe(III) *Ph*-2/2HbO (*symbols* are the same as those used in the *middle panel*). *Continuous lines* show nonlinear least-squares fits to data employing Eq. S1 (see the ESM) and parameters reported in Table 2; *dashed lines* show nonlinear least-squares fits to data employing Eq. 3

Table 2 Kinetic parameters for azide binding to bimolecular species of Fe(III) *Ph*-2/2HbO (indicated as *r*1 and *r*2) at pH 7.0 and 20 °C, according to Scheme S1, employing Eq. S1 (see the ESM)

	*r*1	*r*2
k_1 (s^{-1})	$1.0\ (\pm 0.2) \times 10^3$	$3.6\ (\pm 0.5) \times 10^1$
k_2'/k_1' (M^{-1})	0.23 ± 0.04	1.2 ± 0.3
k_2 (s^{-1})	2.4 ± 0.4	0.07 ± 0.01

hidden by the bands of the other two species at $g \sim 2.2$ or by the spurious band.

The g tensor anisotropy of these LS forms is typical of N and O ligation to the heme (Table 3) [5, 20, 35–41]. The Blumberg–Peisach diagram [36] can provide some empirical guidance to obtain an indication of possible LS heme iron axial ligands, although it should be kept in mind that a number of pitfalls have been found in the use of this diagram, and it should not be used as the only criterion for ligand assignment [42]. The rhombicity (V/Δ) and tetragonality (Δ/λ) parameters determined from the g values [43, 44] of the predominant LS form at pH 7.6 (form 1; $V/\Delta = 0.59$, $\Delta/\lambda\pm = 3.30$) place it in the H-type group of the Blumberg–Peisach diagrams [36], characterized by systems with bis-His axial coordination. Nevertheless, the g values of form 1 are quite similar to those of the human serum albumin–ibuprofen complex (2.93, 2.27, 1.55), which is characterized by His–Fe–Tyr axial coordination [41] (Table 3). A similar assignment to the H group of the Blumberg–Peisach diagram was also reported for the HasA proteins from *S. marcescens* and *P. aeruginosa* at neutral pH ($g = 2.86$, 2.21, 1.71), which are characterized by His–Fe–Tyr axial coordination. It is noted that the original EPR study of *S. marcescens* HasA, prior to the determination of the crystal structure, mistakenly assigned a bis-His axial heme coordination [39, 40]. Furthermore, the rhombicity and tetragonality crystal parameters determined from the g values of *Chlamydomonas* Hb, which is assigned to His–Fe–Tyr axial coordination [20], place it in the H structural group [20]. In all the cited cases, the tyrosinate ligand is

form 1, $g = 2.95$, 2.28, 1.49, form 2, $g = 2.51$, ~ 2.29, 1.86, and form 3, $g = 2.77$, −, 1.63 (Table 3). The g values reported for form 2 should be considered to be average values, as at each g value there is evidence of more than one species with very similar g values, likely indicative of some structural flexibility at this site (see Fig. S7 of the ESM). The band corresponding to g_2 of form 3 is likely

Table 3 Comparison of the EPR spectral parameters of various low-spin heme proteins

Protein	g_1	g_2	g_3	pH	Coordination	Reference
Ph-2/2HbO	2.95	2.28	1.49	7.6	His/Tyr⁻ [a]	This work
Ph-2/2HbO	2.51	∼2.29	1.86	7.6	His/Tyr⁻	This work
Ph-2/2HbO	2.77	–	1.63	7.6	His/Tyr⁻ [a]	This work
HRPA2	2.96	2.13	1.66	Alkaline	His/OH⁻ [a]	[35]
Mb	2.55	2.17	1.85	Alkaline	His/OH⁻	[5]
L. pectinata Hb II	2.61	2.20	1.82	Alkaline	His/OH⁻	[5]
Various heme proteins[b]	∼2.8	2.4	1.5		His/His	[36, 37]
Cytochrome *b*	>3				His/His[c]	[38]
Chlamydomonas Hb	2.52	2.31	1.86	Alkaline	His/Tyr⁻ [a]	[20]
S. marcescens HasA	2.85	2.21	1.71	7.5	His/Tyr⁻ [a]	[39, 40]
HSA ibuprofen	2.93	2.27	1.55	6.9	His/Tyr⁻ [a]	[41]
L. pectinata Hb II	2.76	2.20	1.75	Alkaline	His/Tyr⁻	[5]
HH cytochrome *c*	3.06	2.25	1.25	7.0	Met/His	[37]
Euglena cytochrome	3.20	2.05	1.39	7.0	Met/His[d]	[37]
HH cytochrome *c*	3.37	2.1		Alkaline	Lys/His	[37]
HH cytochrome *c*	3.58			Alkaline	Lys/Lys	[37]

HRPA₂ horseradish peroxidase isoenzyme A₂, *HSA* human serum albumin, *HH* horse heart

[a] OH⁻ strongly H-bonded

[b] Approximate *g* values

[c] Imidazole planes, nonparallel

[d] Imidazole with enhanced H-bonding

strongly H-bonded with a nearby residue, which has been suggested to be the origin of the atypical crystal field parameters for O heme ligation [20, 40]. Hence, by analogy with these three cases, form 1 is proposed to be a tyrosinate LS heme species that is strongly H-bonded with a neighboring residue.

The crystal field parameters of form 2 ($V/\Delta = 0.82$, $\Delta/\lambda = 5.17$) are consistent with normal O coordination of the heme based on the Blumberg–Peisach diagram [36]. Thus, it is suggested that in this case the bound Tyr residue is not involved in H-bonding interactions and, consequently, is deprotonated. It cannot be completely excluded that form 2 corresponds to His–Fe–OH⁻ coordination (see Table 3), although this possibility is considered unlikely as there is no evidence for a hydroxyl complex in the UV–vis spectrum at 12 K at pH 7.6 (Fig. 1a) [23]. The heme coordination of form 3 ($g_1 = 2.77$, –, 1.63) is uncertain due to the absence of g_2; however, the g tensor anisotropy suggests a probable assignment to the H group of the Blumberg–Peisach diagram and, therefore, bis-His coordination. This can be ruled out, as there are no histidine residues in the near vicinity of the distal heme pocket of *Ph*-2/2HbO, suggesting that the coordination is His–Fe–Tyr, with the tyrosinate ligand involved in a H-bonding interaction with neighboring resides distinct from that of form 1. Thus, in accord with the UV–vis and RR data, all of the LS forms are assigned to His–Fe–Tyr heme coordination.

The apparent absence in the RR spectrum of a third LS form observed in the EPR spectrum at 5 K is likely due to two forms having very similar RR frequencies.

Molecular dynamics simulations

The most stable structure found by homology modeling was used to perform 40 ns of MD simulations. To elucidate the potential residue(s) involved in the hexacoordinated conformation, we monitored selected key distances during the simulation. As reported for other Group II Hbs, the oxygen atom of TyrB10 was found to be close to the Fe(III) atom [16, 20]. However, TyrCD1 was found to be even closer to the Fe(III) atom than TyrB10 (Fig. 4). This is the first reported case in which the TyrCD1 may be bound to the Fe(III) atom.

On this basis, we constructed two models in which either TyrCD1 or TyrB10 was coordinated to the Fe(III). MD simulations of these models were performed in order to determine the stabilities of these potential structures. The results show that both systems were stable during the 20 ns of the MD (see Figs. S8, S9 of the ESM). We also found that when TyrCD1 is coordinated to the iron atom, TrpG8 is H-bonded to the O⁻ of TyrCD1, highlighting the important role of this residue (Fig. 5). On the other hand, when TyrB10 is coordinated to the iron, both TrpG8 and TyrCD1 are H-bonded to the O⁻ of TyrB10 (Fig. 6). These
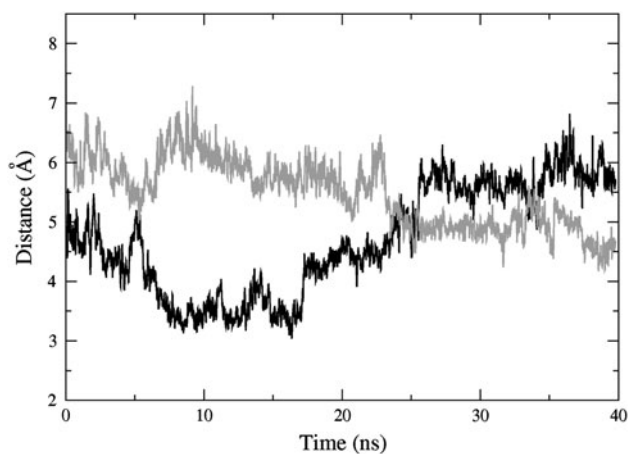
Fig. 4 *Ph*-2/2HbO Fe(III). Time evolution of selected distances between distal residues of the protein. The distances are defined as the distances between the iron and the hydroxylic oxygen of TyrCD1 (*black*), or the iron and the hydroxylic oxygen of TyrB10 (*dark gray*)

results are fully in keeping with the presence of multiple LS forms displaying different heme binding affinities and spectroscopic properties.

Discussion

Unlike the great majority of bacteria, *Ph*TAC125 possesses three genes encoding 2/2 Hbs, two of which belong to Group II, and one gene encoding flavoHb. Sequence alignment (Fig. S2 of the ESM) of *Ph*-2/2HbO with other 2/2 Hbs indicates that the conserved residues HisF8, TyrB10, TrpG8, TyrCD1, IleE7, and PheE11 are at the typical positions for Group II Hbs [17, 18]. On the proximal side, HisF8 is coordinated to the heme iron, as confirmed by the ν(Fe–Im) stretching mode at 223 cm^{-1} in the RR spectrum of the deoxy form (data not shown).

Ph-2/2HbO presents an unusual extension of 15 residues at the N-terminus (pre-A helix). A similar situation had also been found in *M. tuberculosis* HbN (Group I) and appears to occur in many slow-growing species of mycobacterium, such as *M. bovis*, *M. avium*, *M. microti*, *M. marinum* [45], and *S. oneidensis* [18]. The X-ray structure of *M. tuberculosis* HbN (1IDR) showed that the pre-A motif does not significantly contribute to the structural integrity of the protein, protruding out of the compact globin fold, but rather confers a vital contribution in regulating the efficient nitrogen-monoxide-dioxygenase activity of HbN [45].

Inactivation of the *Ph*-2/2HbO encoding gene makes the mutant bacterial strain sensitive to high oxygen pressure, to H$_2$O$_2$ and to nitrosating agents, suggesting a potential role of the protein in oxidative and nitrosative stress [46].
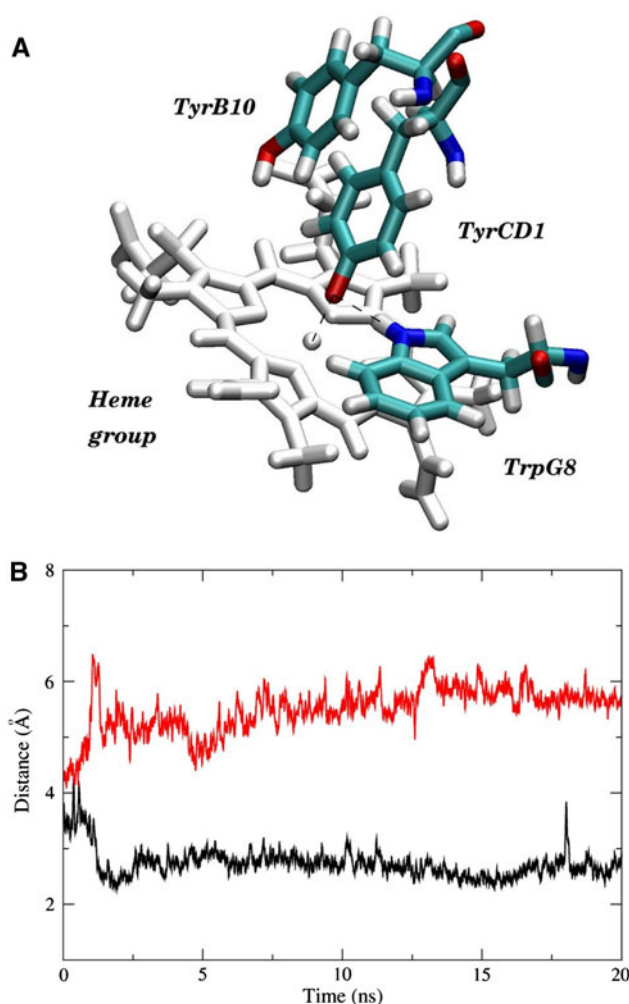
Fig. 5 *Ph*-2/2HbO with TyrCD1-O$^-$ coordinated to the heme iron. **a** Schematic representation of the distal site of the protein showing the coordinated TyrCD1-O$^-$ stabilized by a H-bond with the TrpG8. As shown in **b**, the distance between TyrCD1-O$^-$ and the hydroxylic proton of TyrB10 is too long to form a H-bond. **b** Time evolution of selected distances between the O$^-$ atom of the coordinated TyrCD1 and the indole Nε proton of TrpG8 (*black*), and the hydroxylic proton of TyrB10 (*red*)

At neutral pH, the heme population of *Ph*-2/2HbO contains a mixture of 6cHS (aquo) and different 6cLS heme forms. The LS forms are all characterized by a nonprotonated tyrosinate bound to the heme iron, which experience different degrees of H-bonding with neighboring H-bond donors. Either TyrCD1-O$^-$ or TyrB10-O$^-$ are suggested to be coordinated to the heme Fe(III) atom. The first residue is stabilized by TrpG8 and the second by both TrpG8 and TyrCD1. Clearly, TrpG8 plays a very important role in the stabilization of the coordinated tyrosyl residues. The lower redox potential of *Ph*-2/2HbO at pH 7.0 (i.e., −80 mV vs. SHE) compared to that of horse heart Mb and human Hb (+50 and +135 mV, respectively) [19] does indeed agree with the presence of Tyr as axial ligand.
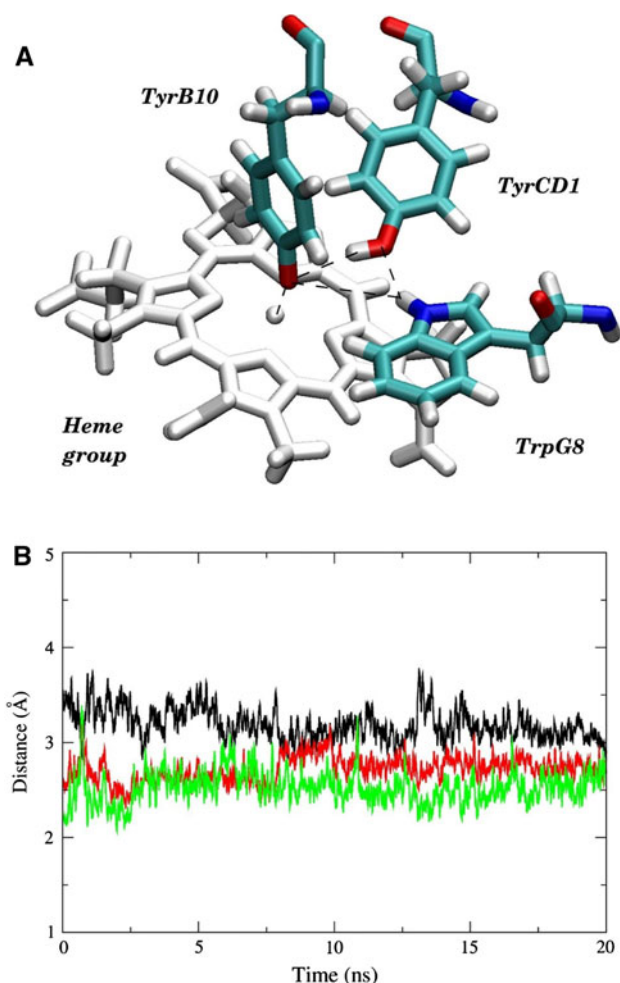
Fig. 6 *Ph*-2/2HbO with TyrB10-O$^-$ coordinated to the heme iron.
a Schematic representation of the distal site of the protein, showing
the coordinated TyrB10-O$^-$ stabilized by H-bonds with both TyrCD1
and TrpG8. Interaction between TyrCD1 and TrpG8 is also indicated.
b Time evolution of selected distances between the TyrB10-O$^-$ atom
with the indole Nε proton of TrpG8 (*black*), the TyrB10-O$^-$ atom
with the hydroxylic proton of TyrCD1 (*red*), and the indole Nε proton
of TrpG8 with the hydroxylic oxygen of TyrCD1 (*green*)

Moreover, the kinetic behavior observed for azide binding
indicates the presence of three reacting forms, suggesting
that the HS and LS hexacoordinated forms do not inter-
change quickly. The faster component displays a fairly fast
dissociation rate (likely corresponding to the hexacoordi-
nated HS species with a water molecule coordinated to the
heme), even faster than those reported for water dissocia-
tion from Mbs [47, 48]. The slight redshift of the CT1 in
Ph-2/2HbO compared to Mbs [48] suggests that this feature
might be accounted for by the lack of a H-bond between
the water molecule and distal residues of the heme pocket.
Thus, in Mbs the water molecule is H-bonded with distal
His that stabilizes the Fe(III)–H$_2$O interaction, slowing
down its dissociation rate; this H-bonding is not present (or

is much weaker) in the distal pocket of *Ph*-2/2HbO, ren-
dering the water dissociation much faster. The slower
bimolecular component is characterized by a very slow
dissociation rate of the hexacoordinating ligand (Table 2),
a behavior that is in keeping with a stronger interaction
between this endogenous ligand (possibly one of the two
Tyr residues, TyrCD1 or TyrB10) and the heme. The
slowest azide-independent rate constant could instead
correspond to a form where the hexacoordination by Tyr is
stabilized by the H-bond network mentioned above.

All of the results presented here indicate that *Ph*-2/
2HbO displays unique adaptive structural properties con-
ferring higher flexibility to the protein that may facilitate
the functioning in the cold by providing greater freedom
for the correct positioning of ligand(s), even at low tem-
peratures. Alternatively, the multiple hexacoordinated
states may account for multiple functions in the same
molecule. Hexacoordinated Hbs are observed in unicellular
eukaryotes [17], plants [49], invertebrates [50], and in
some tissues of higher vertebrates [48, 51], but only a few
cases have been examined and reported in the literature for
bacterial 2/2 Hbs [52–55]. The physiological role of these
hexacoordinated Hbs is not well understood. Several roles
have been suggested for them: oxygen scavengers under
hypoxic conditions [56, 57], terminal oxidases [58], oxy-
gen sensors [59, 60], and that they are involved in nitrogen
monoxide metabolism [61].

The discovery of hexacoordinated neuroglobin and
cytoglobin in man and other vertebrates suggests that in
different phylogenetically unrelated groups of organisms,
these proteins may be endowed with a common function
that is mainly linked to the production of reactive oxygen
species (ROS) and nitrogen monoxide. The sixth ligand is
usually provided by the imidazole side chain of a His,
normally present at the distal site of the heme pocket, and
only a few examples have been reported where TyrB10 has
been found to act as the sixth ligand at the iron site in the
ferrous [55] and ferric states [16, 20]. Indeed, the amino-
acid sequence, the MD simulations, and the spectroscopic
data of *Ph*-2/2HbO indicate that the distal ligands of the LS
ferric form can be either TyrCD1 or TyrB10.

In summary, the existence of several similar LS forms
suggests that the protein has a high degree of structural
flexibility that gives rise to conformers which may be
distinguished by the strength of the H-bond interactions
with the Tyr ligand and/or the disposition of the H-bonding
partner.

References

1. Deming JW (2002) Curr Opin Microbiol 5:301–309
2. Médigue C, Krin E, Pascal G, Barbe V, Bernsel A, Bertin PN, Cheung F, Cruveiller S, D'Amico S, Duilio A, Fang G, Feller G, Ho C, Mangenot S, Marino G, Nilsson J, Parrilli E, Rocha EP, Rouy Z, Sekowska A, Tutino ML, Vallenet D, von Heijne G, Danchin A (2005) Genome Res 15:1325–1335
3. Giordano D, Parrilli E, Dettaï A, Russo R, Barbiero G, Marino G, Lecointre G, di Prisco G, Tutino ML, Verde C (2007) Gene 398:69–77
4. Nicoletti FP, Comandini A, Bonamore A, Boechi L, Boubeta F, Feis A, Smulevich G, Boffi A (2010) Biochemistry 49:2269–2278
5. Kraus DW, Wittenberg JB, Lu JF, Peisach J (1990) J Biol Chem 265:16054–16059
6. Brittain T, Yosaatmadja Y, Henty K (2008) IUBMB Life 60:135–138
7. Ferri T, Poscia A, Santucci R (1998) Bioelectrochem Bioenerg 44:177–181
8. Nicoletti FP, Thompson M, Howes BD, Franzen S, Smulevich G (2010) Biochemistry 49:1903–1912
9. Sali A, Blundell TL (1993) J Mol Biol 234:779–815
10. Tatusova TA, Madden TL (1999) FEMS Microbiol Lett 174:247–250
11. Thompson JD, Gibson TJ, Plewniak F, Jeanmougin F, Higgins DG (1997) Nucleic Acids Res 25:4876–4882
12. Pearlman DA, Case DA, Caldwell JW, Ross WS, Cheatham TE, Debolt S, Ferguson D, Seibel G, Kollman P (1995) Comput Phys Commun 91:1–41
13. Boechi L, Martí MA, Milani M, Bolognesi M, Luque FJ, Estrin DA (2008) Proteins 73:372–379
14. Boechi L, Manez PA, Luque FJ, Marti MA, Estrin DA (2010) Proteins 78:962–970
15. Marti MA, Capece L, Bidon-Chanal A, Crespo A, Guallar V, Luque FJ, Estrin DA (2008) Methods Enzymol 437:477–498
16. Milani M, Pesce A, Nardini M, Ouellet H, Ouellet Y, Dewilde S, Bocedi A, Ascenzi P, Guertin M, Moens L, Friedman JM, Wittenberg JB, Bolognesi M (2005) J Inorg Biochem 99:97–109
17. Wittenberg JB, Bolognesi M, Wittenberg BA, Guertin M (2002) J Biol Chem 277:871–874
18. Vuletich DA, Lecomte JT (2006) J Mol Evol 62:196–210
19. Antonini E, Brunori M (1971) Hemoglobin and myoglobin in their reactions with ligands. North-Holland, Amsterdam
20. Das TK, Couture M, Lee HC, Peisach J, Rousseau DL, Wittenberg BA, Wittenberg JB, Guertin M (1999) Biochemistry 38:15360–15368
21. Caillet-Saguy C, Turano P, Piccioli M, Lukat-Rodgers GS, Czjzek M, Guigliarelli B, Izadi-Pruneyre N, Rodgers KR, Delepierre M, Lecroisey A (2008) J Biol Chem 283:5960–5970
22. Alontaga AY, Rodriguez JC, Schonbrunn E, Becker A, Funke T, Yukl ET, Hayashi T, Stobaugh J, Moenne-Loccoz P, Rivera M (2009) Biochemistry 48:96–109
23. Smulevich G, Miller MA, Kraut J, Spiro TG (1991) Biochemistry 30:9546–9558
24. Smulevich G, Wang Y, Edwards SL, Poulos TL, English AM, Spiro TG (1990) Biochemistry 29:2586–2592
25. Smulevich G, Paoli M, Burke JF, Sanders SA, Thorneley RNF, Smith AT (1994) Biochemistry 33:7398–7407
26. Smulevich G, Feis A, Focardi C, Tams J, Welinder KG (1994) Biochemistry 33:15425–15432
27. Que L (1988) Metal-tyrosinate proteins. In: Spiro TG (ed) Biological applications of Raman spectroscopy, vol 3. Wiley, New York, pp 491–521
28. Hu S, Smith KM, Spiro TG (1996) J Am Chem Soc 118:12638–12646
29. Nagai K, Kagimoto T, Hayashi A, Taketa F, Kitagawa T (1983) Biochemistry 22:1305–1311
30. Nagai M, Yoneyama Y, Kitagawa T (1989) Biochemistry 28:2418–2422
31. Adachi S, Nagano S, Ishimori K, Watanabe Y, Morishima I, Egawa T, Kitagawa T, Makino R (1993) Biochemistry 32:241–252
32. Liu Y, Moënne-Loccoz P, Hildebrand DP, Wilks A, Loehr TM, Mauk AG, Ortiz de Montellano PR (1999) Biochemistry 38:3733–3743
33. Eakanunkul S, Lukat-Rodgers GS, Sumithran S, Ghosh A, Rodgers KR, Dawson JH, Wilks A (2005) Biochemistry 44:13179–13191
34. Aki Y, Nagai M, Nagai Y, Imai K, Aki M, Sato A, Kubo M, Nagatomo S, Kitagawa T (2010) J Biol Inorg Chem 15:147–158
35. Howes BD, Feis A, Indiani C, Marzocchi MP, Smulevich G (2000) J Biol Inorg Chem 5:227–235
36. Blumberg WE, Peisach J (1971) Probes of structure and function of macromolecules and membranes. In: Chance B, Yonetani T, Mildvan AS (eds) Probes of enzymes and hemoproteins. Academic, New York, pp 215–228
37. Brautigan DL, Feinberg BA, Hoffman BM, Margoliash E, Peisach J, Blumberg WE (1977) J Biol Chem 252:574–582
38. Walker FA, Huynh BH, Scheidt WR, Osvath SR (1986) J Am Chem Soc 108:5288–5297
39. Izadi N, Henry Y, Haladjian J, Goldberg ME, Wandersman C, Delepierre M, Lecroisey A (1997) Biochemistry 36:7050–7057
40. Arnoux P, Haser R, Izadi N, Lecroisey A, Delepierre M, Wandersman C, Czjzek M (1999) Nat Struct Biol 6:516–520
41. Nicoletti FP, Howes BD, Fittipaldi M, Fanali G, Fasano M, Ascenzi P, Smulevich G (2008) J Am Chem Soc 130:11677–11688
42. Teixeira M, Campos AP, Aguiar AP, Costa HS, Santos H, Turner DL, Xavier AV (1993) FEBS Lett 317:233–236
43. Palmer G (1985) Biochem Soc Trans 13:548–560
44. Taylor CPS (1977) Biochim Biophys Acta 491:137–149
45. Lama A, Pawaria S, Bidon-Chanal A, Anand A, Gelpí JL, Arya S, Martí M, Estrin DA, Luque FJ, Dikshit KL (2009) J Biol Chem 284:14457–14468
46. Parrilli E, Giuliani M, Giordano D, Russo R, Marino G, Verde C, Tutino ML (2010) Biochimie 92:1003–1009
47. Coletta M, Angeletti M, De Sanctis G, Cerroni L, Giardina B, Amiconi G, Ascenzi P (1996) Eur J Biochem 235:49–53
48. De Sanctis G, Petrella G, Ciaccio C, Feis A, Smulevich G, Coletta M (2007) Biophys J 93:2135–2142
49. Watts RA, Hunt PW, Hvitved AN, Hargrove MS, Peacock WJ, Dennis ES (2001) Proc Natl Acad Sci USA 98:10119–10124
50. Dewilde S, Ebner B, Vinck E, Gilany K, Hankeln T, Burmester T, Kreiling J, Reinisch C, Vanfleteren JR, Kiger L, Marden MC, Hundahl C, Fago A, Van Doorslaer S, Moens L (2006) J Biol Chem 281:5364–5372
51. Pesce A, Dewilde S, Nardini M, Moens L, Ascenzi P, Hankeln T, Burmester T, Bolognesi M (2004) Micron 35:63–65

52. Visca P, Fabozzi G, Petrucca A, Ciaccio C, Coletta M, De Sanctis G, Bolognesi M, Milani M, Ascenzi P (2002) Biochem Biophys Res Commun 294:1064–1070
53. Scott NL, Falzone CJ, Vuletich DA, Zhao J, Bryant DA, Lecomte JT (2002) Biochemistry 41:6902–6910
54. Falzone CJ, Christie Vu B, Scott NL, Lecomte JT (2002) J Mol Biol 324:1015–1029
55. Razzera G, Vernal J, Baruh D, Serpa VI, Tavares C, Lara F, Souza EM, Pedrosa FO, Almeida FC, Terenzi H, Valente AP (2008) J Biol Inorg Chem 13:1085–1096
56. Burmester T, Weich B, Reinhardt S, Hankeln T (2000) Nature 407:520–523
57. Burmester T, Ebner B, Weich B, Hankeln T (2002) Mol Biol Evol 19:416–421
58. Sowa AW, Guy PA, Sowa S, Hill RD (1999) Acta Biochim Pol 46:431–445
59. Hargrove MS, Brucker EA, Stec B, Sarath G, Arredondo-Peter R, Klucas RV, Olson JS, Phillips GN (2000) Structure 8:1005–1014
60. Kriegl JM, Bhattacharyya AJ, Nienhaus K, Deng P, Minkow O, Nienhaus GU (2002) Proc Natl Acad Sci USA 99:7992–7997
61. Smagghe BJ, Trent JT III, Hargrove MS (2008) PloS ONE 3:e2039